

Frustrated Ostwald Ripening in Self-Assembled Monolayers of Cruciform π -Systems

Gina M. Florio,[⊥] Jennifer E. Klare,^{†,§} Michelle O. Pasamba,^{†,§} Tova L. Werblowsky,^{†,§}
Michelle Hyers,^{†,§} Bruce J. Berne,[†] Mark S. Hybertsen,^{‡,§} Colin Nuckolls,^{*,†,§} and
George W. Flynn^{*,†,§}

Department of Chemistry, Columbia University, New York, New York 10027, Department of Applied Physics/Applied Mathematics, Columbia University, New York, New York 10027, NSF Center for Electron Transport in Molecular Nanostructures (NSEC), Columbia University, New York, New York 10027, and Department of Chemistry, St. John's University, 8000 Utopia Parkway, Jamaica, New York 11439

Received June 14, 2006. In Final Form: September 9, 2006

This study details a scanning tunneling microscopy investigation into the mechanism of chiral grain growth in highly ordered, self-assembled monolayer films composed of cruciform π -systems. Although the molecules themselves are achiral, when they adsorb from solution onto graphite, they adopt a gear-like conformation that, by virtue of the surface, is chiral. These handed subunits arrange themselves into enantiomeric two-dimensional domains. The unique finding from this study is that Ostwald ripening is frustrated between domain boundaries that are of opposite chirality because direct interconversion between the chiral units on the surface is energetically inhibited.

Introduction

Detailed below is a scanning tunneling microscopy investigation into the mechanism of grain growth in highly ordered, self-assembled monolayer films composed of cruciform π -systems (1–4) (Figure 1A).^{1,2} Although the molecules themselves are achiral, when they adsorb from solution onto graphite, they adopt a gear-like conformation that by virtue of the surface is chiral (Figure 1B). These handed subunits arrange themselves into enantiomeric two-dimensional domains.^{3–11} Typically, monolayers at the liquid–solid interface evolve over time so that the small grains are consumed by larger domains in a two-dimensional version^{9,11–15} of Ostwald ripening.¹⁶ Monolayers of the cruciform

molecules ripen normally when the boundary is between grains that have the same handedness. The unique finding from this study is that Ostwald ripening is frustrated between domain boundaries that are of opposite chirality. There are other two-dimensional self-assembled systems that show similar frustrated ripening, but they involve strong and directional intermolecular interactions, such as hydrogen bonding, that are not present here.^{10,14,17–22} For the cruciform π -system, the exchange of molecules at a boundary between two domains of opposite handedness involves either complete or partial molecular desorption, a process that is inhibited by strong surface binding and the energy gained by close packing of molecules in each enantiomeric domain.

Results and Discussion

We monitor the coarsening dynamics of the cruciform molecules on graphite using scanning tunneling microscopy (STM) in a phenyloctane solution.^{9,11–15} Figure 2a shows an STM topographic image for 1 that is typical for each of the derivatives (1–4), revealing a well-ordered, monolayer assembly. The bright crosses indicate that the cruciforms are lying parallel to the graphite surface. The two-dimensional unit cell of 1 (2.85 nm \times 1.53 nm with $\gamma = 98.3^\circ$) was determined by Fourier transform autocorrelation analysis of the STM image. The alkyl chains interdigitate as shown in the STM image in Figure 2C. Nearly identical STM images for 2–4 are contained in the Supporting Information (Figure S1). When the molecules adsorb

* Corresponding authors. (G.F.) Phone (212) 854-4162. Fax (212) 854-8336. E-mail: gwfl@columbia.edu. (C.N.) Phone (212) 854-6289. Fax (212) 932-1289. E-mail: cn37@columbia.edu.

[†] Department of Chemistry, Columbia University.

[‡] Department of Applied Physics/Applied Mathematics, Columbia University.

[§] NSEC.

[⊥] St. John's University.

(1) Klare, J. E.; Tulevski, G. S.; Sugo, K.; de Picciotto, A.; White, K. A.; Nuckolls, C. *J. Am. Chem. Soc.* **2003**, *125*, 6030–6031.

(2) Klare, J. E.; Tulevski, G. S.; Nuckolls, C. *Langmuir* **2004**, *20*, 10068–10072.

(3) De Feyter, S.; Gesquiere, A.; Abdel-Mottaleb, M. M.; Grim, P. C. M.; De Schryver, F. C.; Meiners, C.; Sieffert, M.; Valiyaveetil, S.; Mullen, K. *Acc. Chem. Res.* **2000**, *33*, 520–531.

(4) Berg, A. M.; Patrick, D. L. *Angew. Chem., Int. Ed.* **2005**, *44*, 1821–1823.

(5) Mamdouh, W.; Uji-i, H.; Dulcey, A. E.; Percec, V.; De Feyter, S.; De Schryver, F. C. *Langmuir* **2004**, *20*, 7678–7685.

(6) Mamdouh, W.; Uji-i, H.; Gesquiere, A.; De Feyter, S.; Amabilino, D. B.; Abdel-Mottaleb, M. M. S.; Veciana, J.; De Schryver, F. C. *Langmuir* **2004**, *20*, 9628–9635.

(7) Parschau, M.; Romer, S.; Ernst, K. H. *J. Am. Chem. Soc.* **2004**, *126*, 15398–15399.

(8) Wei, Y. H.; Kannappan, K.; Flynn, G. W.; Zimmt, M. B. *J. Am. Chem. Soc.* **2004**, *126*, 5318–5322.

(9) Lim, R.; Li, J.; Li, S. F. Y.; Feng, Z.; Valiyaveetil, S. *Langmuir* **2000**, *16*, 7023–7030.

(10) Gong, J. R.; Lei, S. B.; Wan, L. J.; Deng, G. J.; Fan, Q. H.; Bai, C. L. *Chem. Mater.* **2003**, *15*, 3098–3104.

(11) De Feyter, S.; De Schryver, F. C. *J. Phys. Chem. B* **2005**, *109*, 4290–4302.

(12) Samori, P.; Mullen, K.; Rabe, H. P. *Adv. Mater.* **2004**, *16*, 1761.

(13) Kim, K.; Plass, K. E.; Matzger, A. J. *Langmuir* **2003**, *19*, 7149–7152.

(14) Lackinger, M.; Griessl, S.; Kampschulte, L.; Jamitzky, F.; Heckl, W. M. *Small* **2005**, *1*, 532–539.

(15) Stabel, A.; Heinz, R.; Deschryver, F. C.; Rabe, J. P. *J. Phys. Chem.* **1995**, *99*, 505–507.

(16) We use the terminology “Ostwald ripening” to describe the mechanism for two-dimensional coarsening.

(17) Stawasz, M. E.; Sampson, D. L.; Parkinson, B. A. *Langmuir* **2000**, *16*, 2326–2342.

(18) Giancarlo, L. C.; Fang, H.; Rubin, S. M.; Bront, A. A.; Flynn, G. W. *J. Phys. Chem. B* **1998**, *102*, 10255–10263.

(19) Qian, P.; Nanjo, H.; Yokoyama, T.; Suzuki, T. M.; Nanjo, H.; Miyashita, T. *Chem. Commun.* **1998**, *8*, 943–944.

(20) Rabe, J. P.; Buchholz, S. *Science* **1991**, *253*, 424–427.

(21) Venkataraman, B.; Breen, J. J.; Flynn, G. W. *J. Phys. Chem.* **1995**, *99*, 6608–19.

(22) Cyr, D. M.; Venkataraman, B.; Flynn, G. W. *Chem. Mater.* **1996**, *8*, 1600–1615.

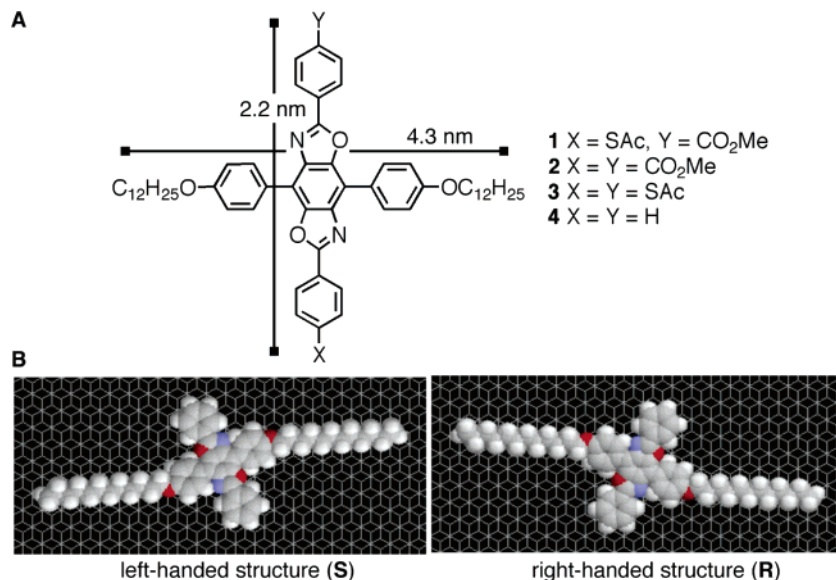


Figure 1. (A) Structure of the gear-shaped, cruciform π -systems with different end groups studied by STM. (B) The geometry optimized structure of **4** on a model graphite surface is chiral with right-handed (R) and left-handed (S) forms.

to the surface, the horizontal plane of symmetry within the molecule is broken (Figure 1B).²³ The molecules adopt either *R* or *S* chirality and assemble into monolayers that are homochiral. Although the molecules themselves are achiral, the domains have a supramolecular chirality upon adsorption.^{3–11,24} In Figure 2A, the rotation of the cruciform molecular core relative to the lamellar axis by 30° is clearly resolved, providing an unambiguous marker of the domain chirality.

The chiral molecular and supramolecular structures observed in the STM images for the assembly of **1–4** are essentially identical to the calculated structures. These structures, shown in Figure 1B, were generated using classical force field calculations and molecular dynamics simulations on a model graphite surface under vacuum conditions.^{25,26} To simplify the calculations, we used the hydrogen-terminated cruciform (**4**). For the individual molecule, we find that the binding energy on graphite is -147 kcal/mol. This energy is largely ($\sim 78\%$) composed of the van der Waals interactions, with the remainder being due to the image charge interactions between the molecule and the surface. The flat conformation on the surface strains the molecule relative to the gas-phase configuration (~ 2 kcal/mol strain energy). The calculated structure for 36 molecules of the hydrogen-terminated cruciform (**4**) on a model graphite surface in a vacuum is shown in Figure 2D. The calculated energy gain upon formation of an ordered assembly is 10 kcal/mol. Whereas the structure agrees with the experimental observation, it also provides a better picture of the location and arrangement of the alkyl chains. The model shows that the spacing between alkyl chains has two characteristic length scales: one at ~ 9 Å (red line in Figure 2D) and another at 4.5 Å (yellow line in Figure 2D). The 4.5-Å spacing is consistent with the ideal packing distance (between 4.2 and 4.6 Å) for alkyl chains lying parallel to the graphite substrate.²⁰ To maximize these relatively short contacts between the alkyl arms of interdigitated molecules, the core adopts a 30° tilt with respect

to the lamella axis. Although the larger spacing suggests that the alkyl chains may have some fluidity, the orientation of the alkyl arms facilitates the packing and contributes to the domain's handedness.

At lower magnification, we observe multiple domains, ranging in area from 400 to 10 000 nm². The domains appear highly dynamic, particularly along the grain boundaries, as expected. A series of consecutive STM images exemplifying the dynamic nature of the boundaries is shown in Figure 3. This series of images was taken some 8 h after deposition, during which time the system was left unperturbed with the tip disengaged. A marker, identified with a white circle in Figure 3, that allows the thermal drift to be controlled and corrected between scans was present in each of these images.

Quantitative analysis³³ of the dynamics in the sequence of images in Figure 3 was performed to determine the area of the ordered domains and of the disordered and "vacant"²⁷ patches. We calculate the surface coverage to be 80% on average. For each image in the sequence in Figure 3, there are two primary domains, labeled 1 and 2, that remain fairly constant in size throughout, while many other small domains grow and disappear around them. Such an observation is not consistent with Ostwald ripening. Coarsening in 2D is characterized by a reduction in the interfacial (line) energy by a decrease in the perimeter-to-area ratio.¹⁵ The perimeter-to-area ratio of the two largest domains (1 and 2) does not vary much over time. If the system exhibited perfect order—a single domain covering the entire 100 nm by 100 nm image—the perimeter-to-area ratio would be 0.04 nm^{-1} .

(27) Vacant of solute molecules, but solvent is likely present.

(28) The size of the domains and degree of polycrystallinity does not vary significantly with time (>24 h). The domains were similarly unaffected by the quality of the graphite used: GE Advanced Ceramics ZYH and ZYB grades and SPI Supplies SPI-2 grade.

(29) Patrick, D. L.; Cee, V. J.; Purcell, T. J.; Beebe, T. P. *Langmuir* **1996**, *12*, 1830–1835.

(30) Gesquiere, A.; Abdel-Mottaleb, M. M.; De Feyter, S.; De Schryver, F. C.; Sieffert, M.; Mullen, K.; Calderone, A.; Lazzaroni, R.; Bredas, J. L. *Chem.—Eur. J.* **2000**, *6*, 3739–3746.

(31) Padowitz, D. F.; Messmore, B. W. *J. Phys. Chem. B* **2000**, *104*, 9943–9946.

(32) Given the unit cell of the monolayer and the surface area of the graphite ($12 \text{ mm} \times 12 \text{ mm}$), it is estimated that $\sim 10^{15}$ molecules are required for complete surface coverage; 10 μL of a 1 mM solution contains $\sim 10^{15}$ molecules.

(33) U.S. National Institutes of Health NIH Image Software; <http://rsb.info.nih.gov/niih-image/>.

(23) The primary achiral feature of the adsorbed cruciform molecule is the alkyl orientation. A secondary achiral feature, the N and O positions in the core of the molecule are not expected to influence the assembly.

(24) Li, C.; Zeng, Q.; Wu, P.; Xu, S.; Wang, C.; Qiao, Y.; Wan, L.; Bai, C. *J. Phys. Chem. B* **2002**, *106*, 13262–13267.

(25) Florio, G. M.; Werblowsky, T. L.; Mueller, T.; Berne, B. J.; Flynn, G. W. *J. Phys. Chem. B* **2005**, *109*, 4520–4532.

(26) Mueller, T.; Werblowsky, T. L.; Florio, G. M.; Berne, B. J.; Flynn, G. W. *Proc. Natl. Acad. Sci. U.S.A.* **2005**, *5315*–5322.

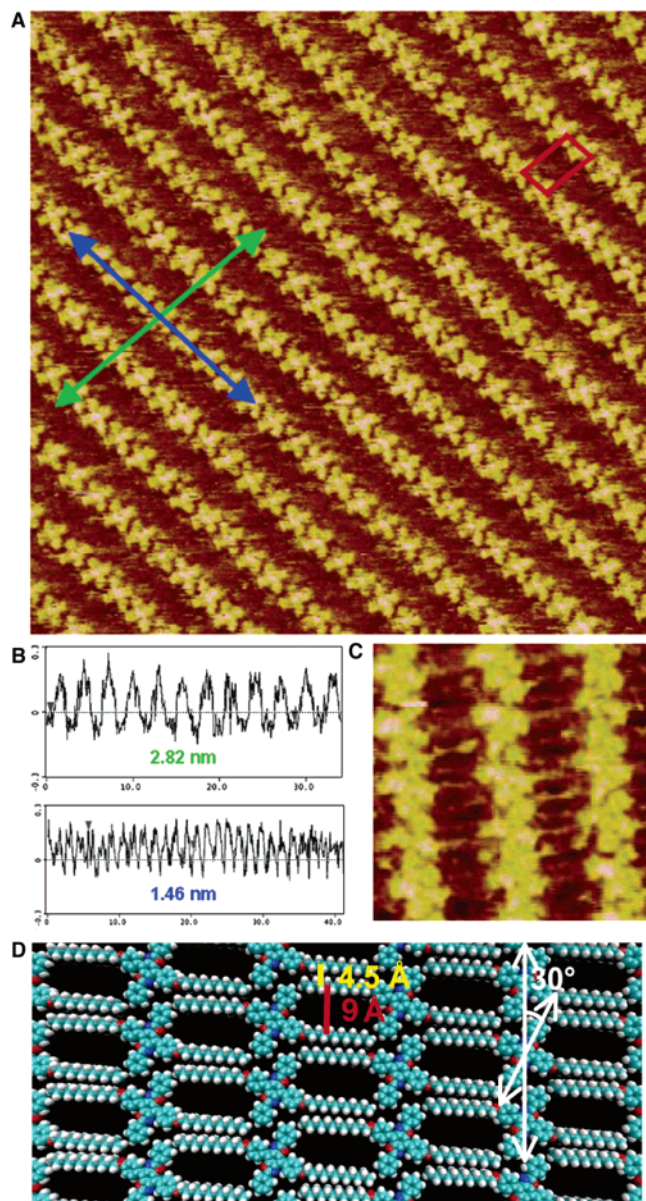


Figure 2. (A) STM topographic image ($30 \text{ nm} \times 30 \text{ nm}$) of cruciform **1** at the 1-phenyloctane-graphite interface obtained at -1.45 V , 45 pA , and 5.5 lines/s in constant current mode. The unit cell parameters ($a = 2.85 \text{ nm}$, $b = 1.53 \text{ nm}$, and $\gamma = 98.3^\circ$), illustrated in red, are deduced from a Fourier transform autocorrelated image. (B) Line profiles taken along the green (top graph) and blue (bottom graph) arrows in the STM image (A) allow a direct measurement of the row spacing (2.82 nm) and the nearest-neighbor distance (1.46 nm). (C) STM image ($10 \text{ nm} \times 10 \text{ nm}$) revealing the interdigitation of the alkyl chains. (D) An optimized structure of 36 molecules of **4** on a model graphite surface forming a macroscopically chiral monolayer.

It is expected that as the surface ripens, the perimeter-to-area ratio of a given domain would decrease and eventually plateau at 0.04 nm^{-1} . The perimeter-to-area ratio for domains 1 and 2 fluctuates around 0.1 nm^{-1} , suggesting that Ostwald ripening is not occurring for these two domains on the time scale of the experiments.

As observed for other systems,²⁰ grain boundaries of the cruciforms are consistently imaged with poor resolution due to the mobility of molecules along these high potential energy edges of the domains. The white arrow in Figure 3, $t = 22 \text{ min}$, indicates such a grain boundary. In contrast, edges of domains neighboring portions of the graphite substrate without adsorbed cruciforms appear crisp and well-resolved (green arrow), suggesting that

these boundaries are of lower potential energy than the ones between cruciform domains. Solvent adsorption along the edge is likely the source of the stabilization because 1-phenyloctane molecules can easily fit into the space between the alkyl chains of neighboring cruciforms.

There are two types of domains in the polycrystalline films that can be designated *R* or *S*, depending on the rotation of the molecules with respect to the lamella axis (either $+30^\circ$ or -30°), as shown in Figure 2D. Other than the different enantiomeric domains, we find no evidence of polymorphism in these samples: the domains are persistent over time²⁸ and unaffected by the presence of the STM tip.²⁹ The angular orientation of the domains with respect to each other does not correspond to epitaxial alignment along the graphite lattice vectors (see Supporting Information, Table S2).^{9, 20}

The domain dynamics and size were very sensitive to the temperature and concentration of the solution.^{30,31} This is shown in Table S3 in the Supporting Information. In general, higher temperatures yielded small domains with numerous voids, and low temperatures gave quantitatively larger domains with no voids. During a given STM experiment, the temperature was held constant to within about $\pm 0.25 \text{ }^\circ\text{C}$. At intermediate concentrations near $1 \times 10^{-5} \text{ M}$, where there are roughly enough molecules to form a complete monolayer,³² we observe the type of grain structure that has holes or open areas in the monolayers, described above for Figure 3 and shown in Figure 4A–D. These submonolayers are a direct consequence of the large surface-binding energy holding the molecules to the substrate. At solution concentrations below $7.5 \times 10^{-6} \text{ M}$, no self-assembly was observed. At concentrations above $1 \times 10^{-5} \text{ M}$ for **1**, we observe one type of grain structure in which domain boundaries are tightly packed adjacent to each other (shown in Figure 5A–C).

The STM images in Figure 4A–C and Figure 5A–C have a serendipitous marker that allows the thermal drift to be controlled and corrected between scans so that a time sequence can be recorded to quantify the degree of homochiral ($S \leftrightarrow S$, $R \leftrightarrow R$) versus heterochiral ($S \leftrightarrow R$) conversion. Color-coded maps showing the change in each domain as a function of time graphically display two different ripening processes, as shown in Figures 4D and 5D. The unchanged portions of the *S* and *R* domains are dark blue and dark green. The interconversion between regions of the same chirality is shown in light green or light blue, and the interconversion between grains of the opposite handedness is shown in the yellow areas. This behavior is tabulated in Table 1 as the change in area or perimeter between the different types of domains.³³ The interconversion of grains when the domains are tightly packed next to each other as in Figure 5 is much slower when the adjacent grains are of opposite handedness than when they are of the same chirality. If the films contain holes or disordered regions at grain boundaries, as in Figure 4, the interconversion becomes significantly faster.

Figure 6 shows a model that offers a possible explanation of how the homochiral and heterochiral interconversion can be so different in films with adjacent grains. The interdigitation of the alkyl arms of the molecules, which lowers the total potential energy of the assembly, results in the gearlike structures shown in Figure 6a. At a boundary between domains of the same chirality, a simple surface translation and rotation can shift a single molecule from registry with one domain into registry with another domain. Although the energy gain per molecule upon assembly is significant (calculated to be 10 kcal/mol for the vacuum-solid interface), at a well-ordered domain boundary, the barrier for shifting a single molecule will be a small fraction of that energy.³⁴

(34) Rabe, J. P.; Buchholz, S. *Phys. Rev. Lett.* **1991**, *66*, 2096–2099.

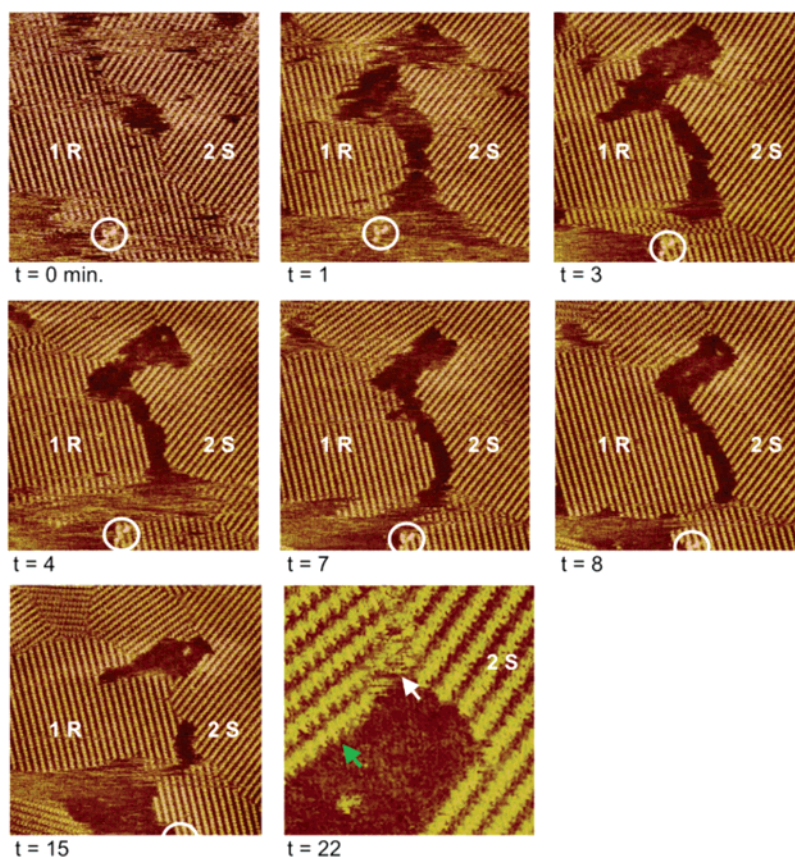


Figure 3. Time sequence ($t = 0$ – 15 min) of STM topographic images of **1** taken over the same $100 \text{ nm} \times 100 \text{ nm}$ area. All images were obtained at -0.5 V , 75 pA , and 6.1 lines/s . The marker is shown in the white circle. The final image ($t = 22$ min) is a higher-magnification micrograph showing a fuzzy interface between grains (white arrow) and a sharp interface with the unresolved solvent molecules (green arrow).

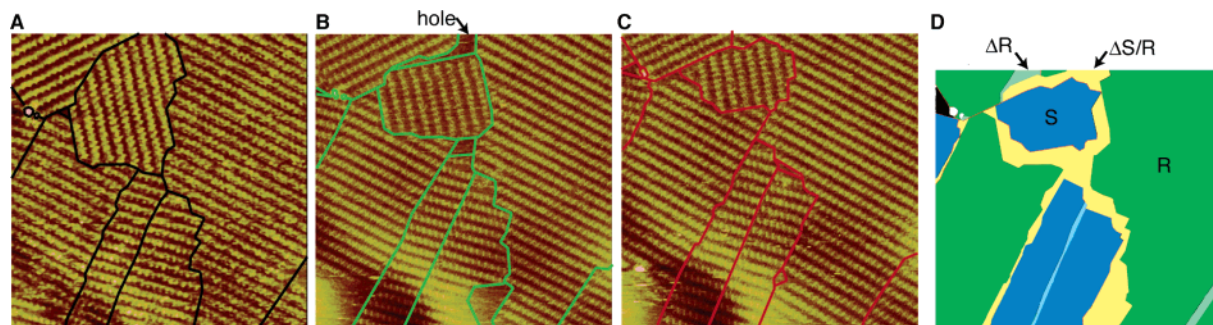


Figure 4. Sequential STM images ($70 \text{ nm} \times 70 \text{ nm}$) for **1** in 1-phenyloctane showing monolayer grain evolution at boundaries that are not tightly packed. (A) $t = 0 \text{ s}$, (B) $t = 2 \text{ min}$, and (C) $t = 4 \text{ min}$. (D) Composite map showing the change in the grain size over time. *S* domains are blue, and *R* domains are green. Regions of *S*-to-*S* conversion are light blue, regions of *R*-to-*R* conversion are light green, and regions of interconversion between *R* and *S* are yellow. Black areas could not be assigned.

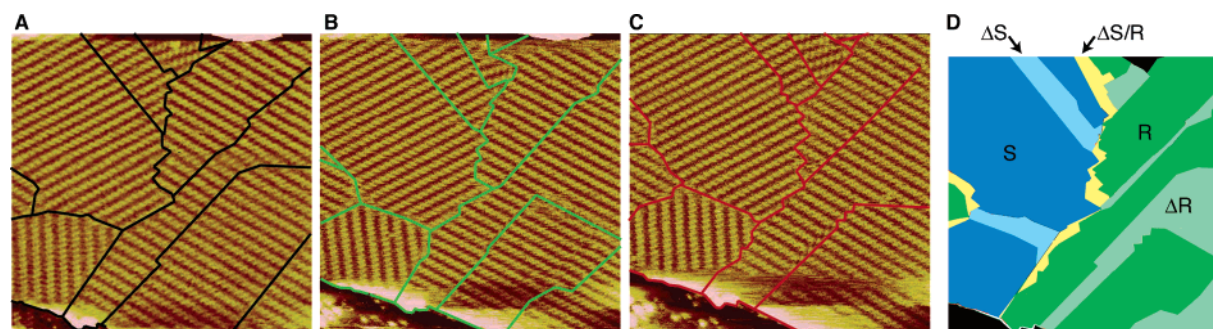


Figure 5. Sequential STM images ($60 \text{ nm} \times 60 \text{ nm}$) for **3** in 1-phenyloctane showing monolayer grain evolution at boundaries that are tightly packed. The notched step in the bottom left is the marker that is used to control the drift. (A) $t = 0 \text{ s}$, (B) $t = 1 \text{ min}$, and (C) $t = 2 \text{ min}$. (D) Composite map showing the change in the grain size over time. *S* domains are blue, and *R* domains are green. Regions of *S*-to-*S* conversion are light blue, regions of *R*-to-*R* conversion are light green, and regions of interconversion between *R* and *S* are yellow. Black areas could not be assigned.

On the other hand, the gearlike meshing of the molecules inhibits transfer of a molecule between domains of opposite chirality (Figure 6B). The incorporation of an *S* molecule (for example)

into an *R* domain is sterically restricted. Conversion must take place prior to incorporation. For a single molecule, conversion between *R* and *S* configurations can follow two pathways. It can

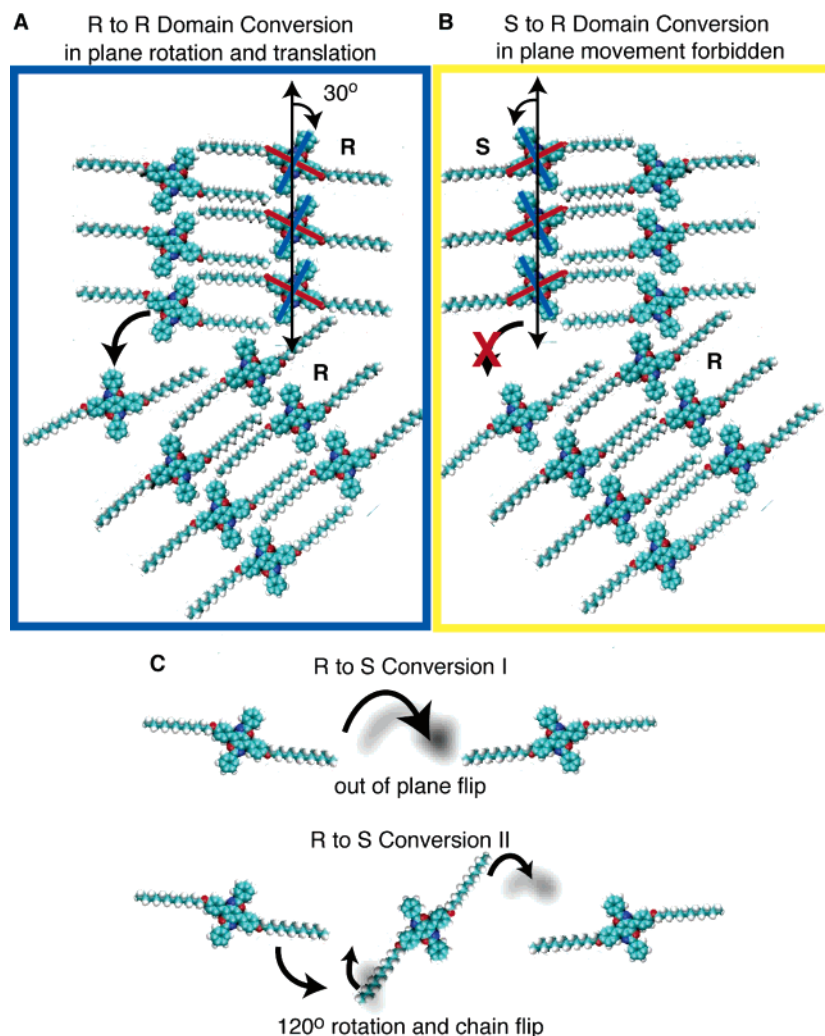


Figure 6. (A) Interconversion between domains of the same chirality requires only an in-plane translation and rotation. (B) Interconversion between domains of opposite chirality is more difficult. (C) To interconvert between domains of opposite chirality requires a complete desorption or in-plane rotation and chain flip (partial desorption).

Table 1. Quantitative Analysis of the Domain Dynamics from Figures 4 and 5

data set	color code	transition	Δ area (nm ²)	Δ perimeter (nm)
Figure 4d ^a	light/dark green	$R \leftrightarrow R$	57	74
	light/dark blue	$S \leftrightarrow S$	29	67
	yellow	$S \leftrightarrow R$	498	246
Figure 5d ^b	light/dark green	$R \leftrightarrow R$	608	311
	light/dark blue	$S \leftrightarrow S$	191	113
	yellow	$S \leftrightarrow R$	82	91

^a The total image area is 4900 nm² (70 nm \times 70 nm). ^b The total image area is 3600 nm² (60 nm \times 60 nm).

undergo a 180° out-of-plane rotation involving complete desorption (Figure 6C). This is essentially indistinguishable from molecular exchange with the supernatant. Alternatively, the molecule can rotate 120° in-plane followed by a reorientation of the alkyl chains (Figure 6C). The second step involves partial lifting of the alkyl chain off of the surface. Calculations of this partial desorption (at the vacuum-solid interface) suggest that the barrier for this process is substantially less than the barrier for full desorption, but still large (~ 38 kcal/mol). Taken together, this explains the facile conversion for heterochiral domains but conversion between enantiomeric domains at close packed boundaries is inhibited. The situation at disordered domain boundaries or open spaces on the surface is more complex; in

part, because it is no longer reasonable to ignore the role of the solvent in the dynamics. Moreover, the solvent could have a role in the supramolecular structure by packing within the spaces between the alkyl arms.

Conclusion

In conclusion, we have demonstrated a hierarchy of assembly properties in a series of cross-shaped molecules at the liquid-graphite interface. At the molecular level, information is encoded that renders the molecules chiral when they adsorb to the surface. The chiral subunits organize themselves into homochiral monolayer domains. This organization creates two distinct types of grain boundaries: ones that are between domains of the same chirality and ones that are between domains of opposite chirality. Interconversion between grains that are of opposite chirality appears to be energetically or temporally inaccessible at close-packed domain boundaries, and Ostwald ripening is thereby frustrated.

Acknowledgment. We acknowledge primary financial support from the Nanoscale Science and Engineering Initiative of the National Science Foundation under NSF Award Number CHE-0117752 and by the New York State Office of Science, Technology, and Academic Research (NYSTAR). C.N. thanks the U.S. National Science Foundation Career award (No. DMR-02-37860), the American Chemical Society PRF type G (No.

39263-G7), the Camille Dreyfus Teacher Scholar Program (2004), and the Alfred P. Sloan Fellowship Program (2004). G.W.F. thanks the U.S. National Science Foundation for support under grant CHE 0352582. J.E.K. thanks the American Chemical Society Division of Organic Chemistry for a Graduate Fellowship sponsored by Organic Syntheses. M.O.P. and M.H. thank the Columbia University NSEC for support through the 2004 and 2005 REU program, respectively. The authors thank Prof. Linda

Doerrler and Prof. Tony Heinz for helpful discussions, and Lorenz Kampschulte for performing the FT autocorrelation.

Supporting Information Available: Additional information as noted in text and discussion of theory of adsorption of hydrogen-terminated cruciform molecules. This material is available free of charge via the Internet at <http://pubs.acs.org>.

LA0617199